Materials Advances

ROYAL SOCIETY OF CHEMISTRY

PAPER

View Article Online
View Journal | View Issue

Cite this: *Mater. Adv.*, 2023, 4, 4965

A smart nanopaper sensor for optical diagnosis of *Helicobacter pylori* infection†

Zeinab Asghari Adib,[a] Amir Reza Sharifi,[a] Mohammad Ali Kiani,[a] Hossein Yousefi,[b] Daniel Horák,[c] Uliana Kostiv,[c] Ali Nabavi-Rad,[d] Abbas Yadegar,[d] Mohammad Yaghoubi-Avini[e] and Hamed Golmohammadi *[af]

Despite a decline in its prevalence, *Helicobacter pylori* (*H. pylori*), as the most common causative agent of chronic gastrointestinal diseases, still infects more than half of the world's population. Although effective, current *H. pylori* infection diagnostic approaches entail some drawbacks and hurdles, including requiring endoscopy and multiple biopsies, harmful chemicals, and expensive and bulky apparatus. Herein, to tackle some of state-of-the-art limitations, we have developed a biocompatible nanosensor for diagnosis of *H. pylori* infection. The developed optical sensor comprises $NaYF_4$:Yb,Er,Lu@PEG-NH_2 upconversion nanoparticles, red cabbage-extracted anthocyanins, and iron oxide nanoparticles embedded within chitin nanopaper. The enzymatic reaction of *H. pylori* urease enzyme with urea, which leads to pH changes, and consequently changes in the pH-dependent fluorescence/color profile of the developed sensor *via* an inner filter effect mechanism, was utilized as a sensing strategy for *H. pylori* infection diagnosis. A portable 3D-printed smartphone-based imaging platform was also fabricated for monitoring the developed sensor. We believe that our developed smart nanosensor can not only potentially be exploited as an ingestible sensor for non-invasive diagnosis of *H. pylori* infection, its therapeutic monitoring, and gastrointestinal pH monitoring, but also provide fresh insights into the development of a variety of innovative ingestible/swallowable sensors for non-invasive gastrointestinal diagnostics.

Received 28th August 2023,
Accepted 17th September 2023

DOI: 10.1039/d3ma00612c

rsc.li/materials-advances

Introduction

Bacterial infections have remained as one of the prevailing and critical global health concerns as they still lead to numerous costly outbreaks along with increasing mortality annually worldwide, chiefly owing to the lack of rapid, reliable, and cost-effective sensing methods/tools for their timely diagnosis.[1,2] Among infectious bacteria, *Helicobacter pylori* (*H. pylori*) is known as one of the most prevalent and perilous bacterial pathogens, infecting over 50% of the world's population.[3,4] *H. pylori* is a fastidious Gram-negative spiral-shaped microaerophilic human pathogenic bacterium that colonizes the gastric mucosa and can survive for a prolonged time in the stomach.[5–7] *H. pylori* produces several enzymes such as urease, oxidase, and catalase, of which the urease plays a crucial role in the survival of the bacterium in gastric media by neutralizing acids in the immediate environment through the hydrolysis of urea into ammonia (NH_3) and carbon dioxide (CO_2).[6,8]

H. pylori infection is involved in various gastric-duodenal diseases and is responsible for 60–100% of peptic and duodenal ulcers, 80% of chronic atrophic gastritis, and 90% of mucosa-associated lymphoid tissue lymphoma.[9] Remarkably, gastric cancer, which is categorized as the sixth commonly diagnosed cancer and the fourth leading factor of cancer death in 2020, is mainly caused by the chronic infection of *H. pylori*.[10,11] Regrettably, a large number of studies conducted, especially in recent years, have underscored the antibiotic-resistant *H. pylori* strains.[12,13] Given the importance of *H. pylori* infection diagnosis, particularly at early stages, and its therapeutic

[a] *Nanosensor Bioplatforms Laboratory, Chemistry and Chemical Engineering Research Center of Iran, 14335-186, Tehran, Iran. E-mail: hamed.golmohammadi@imtek.uni-freiburg.de, golmohammadi@ccerci.ac.ir*
[b] *Laboratory of Sustainable Nanomaterials, Department of Wood Engineering and Technology, Gorgan University of Agricultural Sciences and Natural Resources, Gorgan, 4913815739, Iran*
[c] *Institute of Macromolecular Chemistry, Academy of Sciences of the Czech Republic, Heyrovského nám. 2, 162 06 Prague 6, Czech Republic*
[d] *Foodborne and Waterborne Diseases Research Center, Research Institute for Gastroenterology and Liver Diseases, Shahid Beheshti University of Medical Sciences, Tehran, Iran*
[e] *Departments of Microbiology and Microbial Biotechnology, Faculty of Life Sciences and Biotechnology, Shahid Beheshti University G.C., Tehran, Iran*
[f] *Department of Microsystems Engineering (IMTEK), University of Freiburg, 79110 Freiburg, Germany*

† Electronic supplementary information (ESI) available. See DOI: https://doi.org/10.1039/d3ma00612c

monitoring, to date, several invasive and non-invasive diagnostic methods/tests have been developed for its infection detection.[14,15] Invasive tests (ITs) such as a rapid urease test, histology, culture, and polymerase chain reaction (PCR) are based on the direct detection of the *H. pylori* organism in gastric biopsies, which are obtained through endoscopy. ITs involve timely procedures along with several restrictions and are used as routine tests for *H. pylori* detection, the most important of which are the need for sophisticated apparatus and professional labor to run the tests and analyze the results.[16,17] On the flip side, serology, a stool antigen test (SAT), a urea breath test (UBT), and a *H. pylori* saliva antigen test (HPS) are categorized as non-invasive tests (NITs) for *H. pylori* infection detection. The UBT and SAT are among the most commonly used NITs for *H. pylori* infection detection. The UBT, which relies on the *H. pylori* urease activity, measures the amount of $^{13}CO_2$ or $^{14}CO_2$ in exhaled breath of patients before and after ingestion of ^{13}C or ^{14}C-labeled urea, while the SAT detects *H. pylori*-associated antigens in stool samples utilizing an enzyme immunoassay. Although these diagnostic tests provide non-invasive approaches for *H. pylori* infection detection, they suffer from major hurdles, including poor specificity, sensitivity, and reproducibility, and the use of relatively expensive laboratory equipment as well as harmful and isotopically labeled chemicals.[17–20]

To remedy the above-mentioned impediments to ITs and NITs, during the past few years, biosensors have opened a new avenue for the detection of *H. pylori* biomarkers, mainly utilizing functional nucleic acids, particularly DNAzymes and DNA aptamers as the recognition elements.[21–23] Notwithstanding the high sensitivity, selectivity, and specificity revealed by these biosensors, they still suffer from major shortcomings such as low stability and applicability for *in vivo* testing that hinder their further applications in real media.[24,25]

Herein, aiming to tackle some of the aforementioned obstacles we benefit from the concept of ingestible sensors as a new emerging technology at the cutting edge of biosensing to propose a swallowable nanosensor for non-invasive smart diagnosis of *H. pylori* infection. In recent decades, ingestible sensors have arisen as a fascinating and efficient sensing technology for gastrointestinal (GI) tract health monitoring through which different biological parameters such as enzymes, metabolites, hormones, electrolytes, and microbial communities can be monitored and measured in the digestive system. This technology is built upon the capability of sensors to non-invasively pass along the gut lumen and access the GI tract organs, while providing valuable information about the health status of the GI tract.[26–31]

In the current work, for the first time, a nanosensor has been fabricated *via* embedding an anthocyanin pigment (extracted from red cabbage) and $NaYF_4$:Yb,Er,Lu@PEG-NH_2 upconversion nanoparticles (UCNPs) within magnetic chitin nanofiber (ChNF) paper and employed in combination with smartphone technology for smart diagnosis of *H. pylori* infection. The sensing strategy for *H. pylori* infection diagnosis relies on the enzymatic reaction of *H. pylori* urease with urea and production of ammonia through an inner filter effect (IFE) mechanism that leads to variations in the pH-dependent fluorescence/color profile of the fabricated sensor. In order to utilize our fabricated sensor for *in vitro* monitoring of pH/*H. pylori*, we have also developed a portable smartphone-based imaging platform laser setup (SIS). Regarding the non-toxicity, ease of fabrication, and high efficiency of our developed smart sensor for pH/*H. pylori* monitoring, it is envisioned that it can also be potentially inspiring for the development of innovative ingestible/swallowable sensors amenable to diagnosing and monitoring GI tract diseases and parameters.

Experimental section

Materials and equipment

In all experiments, Milli-Q ultrapure water was used. Hydrochloric acid (37%), sodium hydroxide, urea, ammonia solution (25%), ethanol, pepsin, $FeCl_3{\cdot}6H_2O$ and $FeCl_2{\cdot}4H_2O$ were purchased from Merck, Germany. Normal saline solution was purchased from a local drugstore in Iran. For the production of ChNF paper, industrial hydrochloric acid, sodium hydroxide, hydrogen peroxide, and acetic acid were purchased from Mojalali Co., Iran, and used without further purification.

For the synthesis of UCNPs, YCl_3, $YbCl_3$, $ErCl_3{\cdot}6H_2O$, $LuCl_3$, NH_4F, sodium alendronate, dichloromethane, trifluoroacetic acid, triisopropylsilane, and oleic acid were purchased from Sigma-Aldrich (St. Luis, MO, USA). Sodium hydroxide was obtained from Lach-Ner (Neratovice, Czech Republic) and α-amino-ω-Boc-amino PEG (H_2N-PEG-NH-Boc; 5 kDa) was purchased from Rapp Polymere (Tübingen, Germany). The solvents and cellulose dialysis membranes were purchased from Lachema (Brno, Czech Republic) and Spectrum Europe (Breda, Netherlands), respectively.

The UCNP emission spectrum was recorded using an Edinburgh Instruments FS5 spectrofluorometer (Edinburgh, UK) coupled with a CW 980 nm laser diode as an excitation source. The digital images were captured using a Motorola Edge 20 Pro smartphone with the Pro mode. Tecnai Spirit G2 transmission electron microscopy (TEM; FEI; Brno, Czech Republic) and dynamic light scattering (DLS; Scatteroscope I; Qudix, Inc., South Korea) analyses were performed to analyze the shape and size distribution of $NaYF_4$:Yb,Er,Lu nanoparticles. UV-vis absorption spectra were recorded using a spectrophotometer model DR5000TM (Hach, Canada). pH measurements were conducted using a consort C1010 pH meter, United Kingdom. The 3D printing process was carried out using a prusa mark3 slicer, the Czech Republic.

Production of ChNF paper (chitin nanopaper)

As schematically illustrated in Fig. 1A, briefly, the shrimp's shell (Litopenaeus vannamei) was treated first with HCl acid solution (5 wt%) so as to eliminate minerals and further refluxed twice with NaOH solution (5 wt%) for protein elimination. Second, the H_2O_2 solution (0.1 wt%) was utilized to eliminate pigments. Next, a chicken grinder was used to ground the white shells to attain chitin powder. The obtained powder was further converted to 1 wt% chitin suspension and passed through a super disk grinder (MKCA6-3; Masuko Sangyo Co.,

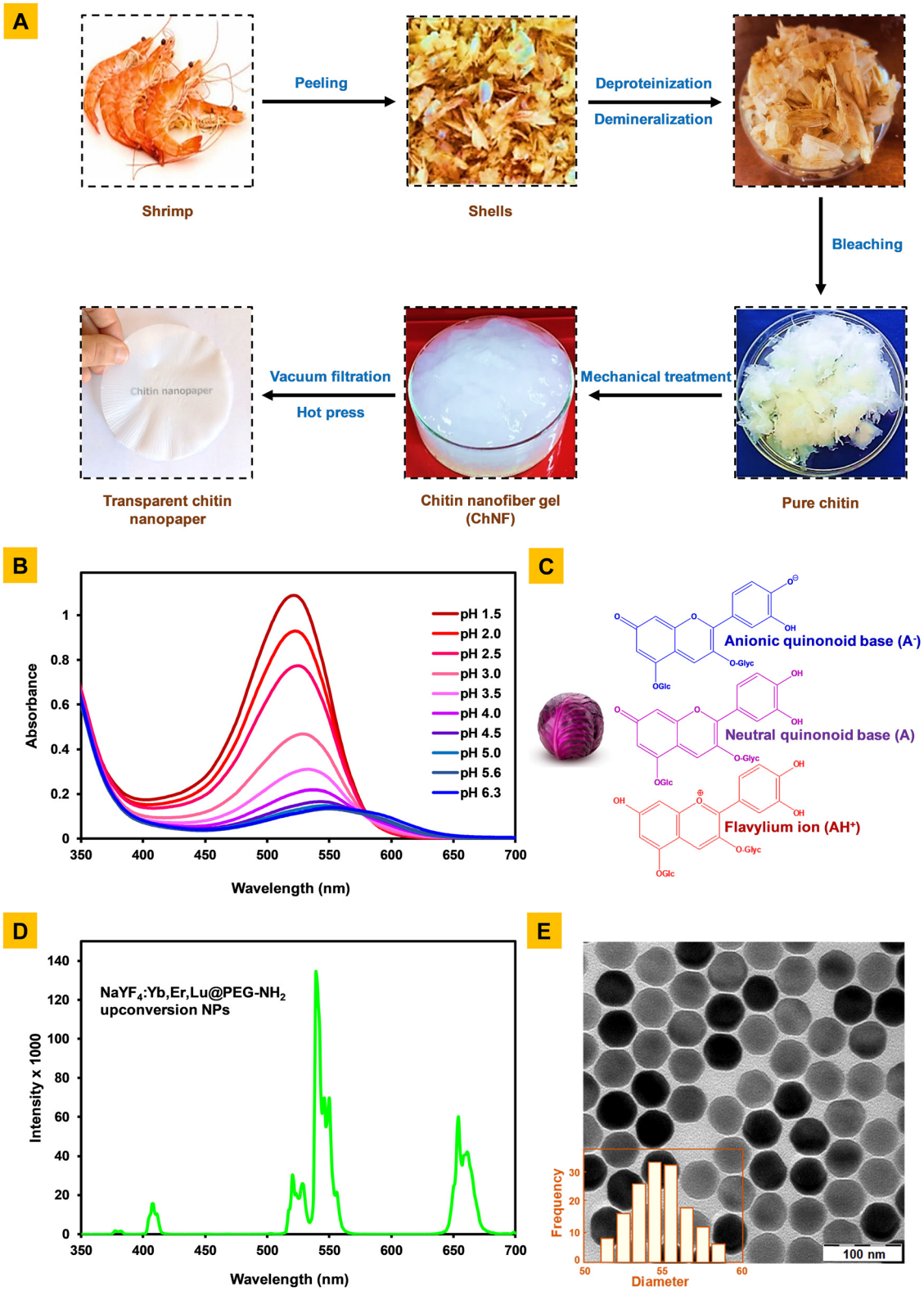

Fig. 1 (A) Experimental steps and production process of the transparent chitin nanopaper from shrimp as a raw material. (B) The absorbance spectra of red cabbage anthocyanins (RCAs) at different pHs (1.5–6.3). (C) The dominant RCA extract structures and colors at different pHs. (D) The PL spectra of $NaYF_4$:Yb,Er,Lu@PEG–NH_2 UCNPs. (E) TEM image of synthesized UCNPs and the attributed DLS analysis.

Ltd) for mechanical nanofibrillation. The chitin suspension was converted to the highly viscous wet gel of ChNF after grinding. The well-dispersed ChNF suspension (0.2 wt%) was filtered by vacuuming followed by hot pressing at 100 °C

and 2 MPa for 1 h. The mentioned process led to the formation of a transparent ChNF paper with a thickness and a density of ~40 μm and 1.1 g cm^{-1}, respectively. Full details of the characterization of the ChNF paper is provided in the ESI.†[32]

Synthesis of UCNPs

The UCNPs were synthesized in a three-step procedure as follows:

Alendronate–PEG–NH_2. With minor modifications of our primarily reported procedure, alendronate–PEG–NH_2 was prepared.[33] Briefly, sodium alendronate (0.032 g) was dissolved in 0.1 M phosphate buffered saline (PBS; 1 mL; pH = 7.4), the solution was cooled to 5 °C, H_2N–PEG–NH–Boc (0.05 g) was added and the mixture was stirred at 5 °C for 12 h and dialyzed (MWCO 3.5 kDa) against water for 5 days; water was exchanged twice a day. After lyophilization, alendronate-PEG-NH-Boc was dissolved in the trifluoroacetic acid/triisopropylsilane/dichloromethane mixture (3 mL/3 mL/30 mL) at ambient temperature for 2 h. After evaporation of dichloromethane, the dry alendronate-PEG-NH_2 product was dissolved in water (5 mL) and the solution was dialyzed (MWCO 3.5 kDa) against water for 5 days (water was exchanged twice a day) and lyophilized.

Synthesis of $NaYF_4$:Yb,Er,Lu nanoparticles. The particles were prepared by modification of a previously described protocol.[34] Briefly, in a 100 mL flask, YCl_3 (94 mg; 0.48 mmol), $YbCl_3$ (56 mg; 0.2 mmol), $ErCl_3{\cdot}6H_2O$ (8 mg; 0.02 mmol), $LuCl_3$ (84 mg; 0.3 mmol), and oleic acid (6 mL) were dissolved in octadec-1-ene (15 mL) and the mixture was heated at 160 °C for 30 min with mild stirring under an argon (Ar) atmosphere. After cooling to ambient temperature, a solution of NH_4F (148 mg; 4 mmol) and NaOH (100 mg; 2.5 mmol) in methanol (5 mL) was added and the mixture was slowly heated to 70 °C under an Ar atmosphere to evaporate methanol and then at 300 °C for 1 h. The resulting $NaYF_4$:Yb,Er,Lu nanoparticles were washed five times with hexane, five times with ethanol/hexane, and four times with ethanol/water (1 : 1 v/v; 15 mL each) using centrifugation (3460 rcf) and redispersion and transferred in water.

PEGylation of $NaYF_4$:Yb,Er,Lu nanoparticles. Ale–PEG–NH_2 (20.5 mg) was added to a dispersion of $NaYF_4$:Yb,Er,Lu nanoparticles (70 mg) in water (6 mL). The mixture was then gently shaken at ambient temperature for 30 h and dialyzed (MWCO 14 kDa) against water for 2 days (water was exchanged twice a day) to remove unreacted alendronate–PEG–NH_2.

Extraction of red cabbage anthocyanins (RCAs)

Approximately, 450 g of fresh red cabbage leaves were chopped into small pieces. Afterward, 240 mL of an ethanol/water solution (7 : 3 v/v) was added to the chopped leaves and the mixture pH was adjusted to 2.0 using HCl (1.0 M). The mixture was then stored at 4 °C for 24 h, while preventing from light. After this, the extract was filtered followed by centrifugation at 4000 rpm for 15 min. The extracted anthocyanin solution was stored at 4 °C in the dark place for further usage.[35]

Synthesis of Fe_3O_4 magnetic NPs

Fe_3O_4 Magnetic NPs were synthesized using a co-precipitation method. Firstly, a mixture of $FeCl_3{\cdot}6H_2O$ and $FeCl_2{\cdot}H_2O$ at a molar ratio of 2 : 1 was prepared in water. Then, 30 mL of concentrated ammonia solution (25%) was added to the prepared solution under vigorous stirring. The mixture was further stirred for 1 h. The resulting Fe_3O_4 NPs were then separated using a strong magnet and washed several times with water and placed at ambient temperature to be dried.[36]

Design and fabrication of magnetic nanopaper-based sensors

First, a concentrated suspension of Fe_3O_4 NPs was prepared in water and one side of circular pieces of ChNF paper (6 mm diameter, cut using a hole puncher) was then casted using the as-prepared suspension in such a way that a crescent shape was created. The ChNF papers were then placed at ambient temperature for ~1 h to be dried. Next, a mixture of the synthesized UCNPs (6 mg mL^{-1}) and RCAs (0.56 mM) was prepared with a volume ratio of 1 : 25. 8 μL of the as-prepared mixture was further dropped on another side of the ChNF paper and allowed for ~30 min to be dried at ambient temperature. Then, the ChNF paper pieces were rinsed with water to remove any non-immobilized reagents. Fig. 3A shows the schematic procedure of nanopaper-based sensor fabrication.

Design and fabrication of a portable smartphone-based imaging platform laser setup (SIS)

In order to design a portable smartphone-based imaging platform equipped with a laser setup, the SolidWorks 2020 program was used. The main compartments of the fabricated imaging platform are composed of an infrared laser diode module (980 nm, input power supply: AC 100–240 V, 1.0 A, 50/60 Hz, output power: 400 mW, class: IIIa and IIIb, beam diameter at aperture: 2.0 mm × 3.5 mm, dimension: D16 mm × L71 mm, Berlin Lasers, China), an optical ultra-violet (UV)/near-infrared (NIR) cut-off filter (ID ~ 50 mm, Iran), and also a glass slide/strip, Iran.

Self-developed android app (IMA)

An android-based mobile app was programmed in Java to analyze the color intensity of the optical sensors in RGB and grayscale color spaces. The app enables the condition in which any saved images in the smartphone can be imported to that. The imported images can be divided into multiple segments for easier color analysis. A pixel-scale input was also coded to cut a specific area of the probes' images, in square, rectangle, or circular shapes without any quality loss. There is no limitation to the number of imported or cut images, however the better the computation capability of the smartphone, the faster the analysis. The developed app autonomously calculates the final concentration of the desired analytes based on the predefined regression equations and color space of each probe. Eventually, the final concentration of each analyte can be stored and transferred *via* any internet-based service such as email services, instant messengers, and cloud services.

Analytical experiments

Gastric juice simulation

For gastric juice simulations, 0.4 g of pepsin was dissolved in 5 mL of HCl (0.1 M), and the mixture was then added to 100 mL of saline solution (0.9% w/v). Eventually, the solution pH was adjusted to the desired pH with HCl/NaOH (1 M).[37]

In vitro detection of pH

To conduct pH detection by using the developed sensor, it was immersed in 3 mL of simulated gastric juice with different pHs ranging from 1.5 to 4.5 and after 10 s its fluorescence/color profile was measured with SIS and subsequently quantified by using IMA.

Bacterial strains and culture

H. pylori clinical strain BY-1 was obtained from the *H. pylori* biobank of Helicobacter Research Laboratory in the Research Institute for Gastroenterology and Liver Diseases, Shahid Beheshti University of Medical Sciences, Tehran, Iran. The isolate was cultured on Brucella agar plates containing 5% sheep blood, 10% fetal calf serum (FCS), the *Campylobacter*-selective supplement (vancomycin 2.0 mg L^{-1}, polymyxin B 0.05 mg L^{-1}, and trimethoprim 1.0 mg L^{-1}), and amphotericin B (2.5 mg L^{-1}) for 2–3 days at 37 °C under microaerophilic conditions (5% O_2, 10% CO_2, and 85% N_2) in a CO_2 incubator (Innova® CO-170; New Brunswick Scientific, USA). Suspensions of *H. pylori* in normal saline were prepared at a density of 9×10^8 CFU mL^{-1} and immediately used in the following experiments.[38]

In vitro detection of *H. pylori*

For *in vitro H. pylori* detection using the developed sensor, it was immersed in 3 mL of simulated gastric juice spiked with *H. pylori* with a total concentration of 10^8 CFU mL^{-1}. Subsequently, the fluorescence/color profile of the developed sensor was imaged using SIS before and 2–3 min after adding 2 μL of urea (1.6 M).

Results and discussion

Nanosensor for the diagnosis of *H. pylori* infection

The developed nanosensor for the diagnosis of *H. pylori* infection comprises UCNPs, RCAs, and Fe_3O_4 NPs immobilized within the 3D scaffold of ChNF paper.

Transparent chitin nanopaper. As a second copious found biopolymer in nature, chitin with a composition of ((1 → 4)-2-acetamido-2-deoxy-β-D-glucan) is the constituent materials of the exoskeletons of crustaceans as well as the cell walls of fungi.[32,39] Chitin endows several promising features, including non-toxicity, abundant nature, affordability, biocompatibility, sustainability, biodegradability, *etc.* As mentioned in Section 2.2, a micrometer-thick sheets of ChNF were high-densified in the form of nanopaper to be used as a compact substrate. Comparing the physiochemical, mechanical and optical features of ChNF with ordinary paper, ChNF paper possesses higher tensile strength under dried and wet conditions, higher aspect ratio, lower porosity, lower permeability to air/water and lower surface roughness, which lead to retaining its structure in aqueous media and harsh conditions. Besides, ChNF paper has higher reactive surface/functional groups because of the existence of hydroxyl and amide groups in its structure. Notably, the inherent structure of ChNF paper alleviates one of the foremost shortcomings in fabricating optical sensors which is the reagent leakage from the surface of the substrate. This situation is underscored principally in the case of ingestible sensors since the sensor experiences a long voyage facing with a complex matrix prior to reaching the intended organ. What's more, the high optical transparency of ChNF is another paramount feature that can affect the performance of optical (bio)sensors, where the use of non-transparent substrates such as paper encounters practical hurdles, especially for *in vivo* monitoring.[40,41]

Upconversion nanoparticles. UCNPs belong to the inimitable category of optical nanomaterials including lanthanide ions, capable of electronic transitions within the 4f electron shells. The usage of low-density NIR light as a nondestructive while highly penetrative excitation source along with the unrivaled anti-Stokes upconversion of lower-energy photons into high-energy ones has brought substantial technological privilege for the usage of UCNPs in different biological and photonic applications, comprising remote neuron modulation, solar energy harvesting, super-resolution imaging/microscopy, light-triggered drug delivery, GI tracing, bioimaging, *etc.*[42–47]

In this work, $NaYF_4$:Yb,Er,Lu@PEG-NH_2 nanoparticles were prepared using a high-temperature co-precipitation method. The mean diameter and height of the synthesized spherocylindrical shape nanoparticles were 55 nm and 41 nm, respectively (Fig. 1E). They were uniform in size and are of great importance for achieving reproducible results in different applications. Also, the luminescence spectrum of the particles showed characteristic green and red emissions (Fig. 1D) of Er^{3+} attributed to the $^2H_{11/2} \rightarrow {}^2I_{15/2}$ (409 nm), $^4S_{3/2} \rightarrow {}^2I_{15/2}$ (525 nm), $^2H_{9/2} \rightarrow {}^4I_{15/2}$ (542 nm), and $^4F_{9/2} \rightarrow {}^2I_{15/2}$ (656 nm) transitions.

It is noteworthy that the reason for introducing a PEG protective coating on the particle surface was to prevent dissolution, reduce the possible toxicity, and maintain the luminescence of the $NaYF_4$:Yb,Er,Lu nanoparticles. We have already evaluated the *in vitro* cytotoxicity of the synthesized UCNPs using primary fibroblasts and cervical carcinoma HeLa cell lines, proving that they do not show significant toxicity even at high concentrations.[34]

Red cabbage anthocyanins. Anthocyanins are a group of naturally occurring phytochemicals responsible for the blue-red colors of many flowers, vegetables, and fruits. RCAs as natural pigments with the pH-dependent nature exhibit diverse color variations at different pH levels on the basis of hyperchromic and bathochromic effects.[48,49] At pH levels lower than 3.0, cationic flavilium with a red color is the most dominant form of RCAs. With the pH increasing to 6.0, the structure of RCAs alters from a cationic flavylium to a neutral quinonoidal

base with a purple color. By increasing the pH to 7.0 and above, the anionic and neutral quinonoidal bases (with blue color) and neutral and anionic chalcones (with green color) are formed, respectively. The extraordinary pH stability of the color of RCAs is believed to be due to the existence of acyl groups, which hinder the hydrolysis of the red flavylium cation to the colorless carbinol base.[50] The absorbance spectra and dominant RCA extract structures at different pH ranges are depicted in Fig. 1B and C, respectively. In this work, the concentration of the RCA extract was estimated to be 0.56 mM based on the Wrolstad method.[51,52]

Fe_3O_4 nanoparticles. The aim of this work is to fabricate a low cost, non-toxic, and easy-to-fabricate/use optical nanosensor capable of potentially being exploited as an ingestible sensor for on-body and non-invasive monitoring of gastric pH/*H. pylori* infection. In this regard, controlling the ingestible sensor motion and its orientation/direction throughout the GI tract to reach the desired organ (herein the stomach) as well as fixing its precise location to be easily monitored by our fabricated imaging platform would be a significant challenging issue. To address this concern, Fe_3O_4 NPs were utilized to achieve a magnetic nanopaper sensor that can be easily controlled by external magnetic forces. This ensures that the developed ingestible sensor is fixed at the desired location to initiate the imaging/monitoring process using our fabricated imaging platform.

A portable smartphone-based imaging platform laser setup for optical monitoring

As shown in Fig. 2A, a 3D-printed dark chamber (181 mm × 129 mm × 10 mm), with explicit places for an adjustable

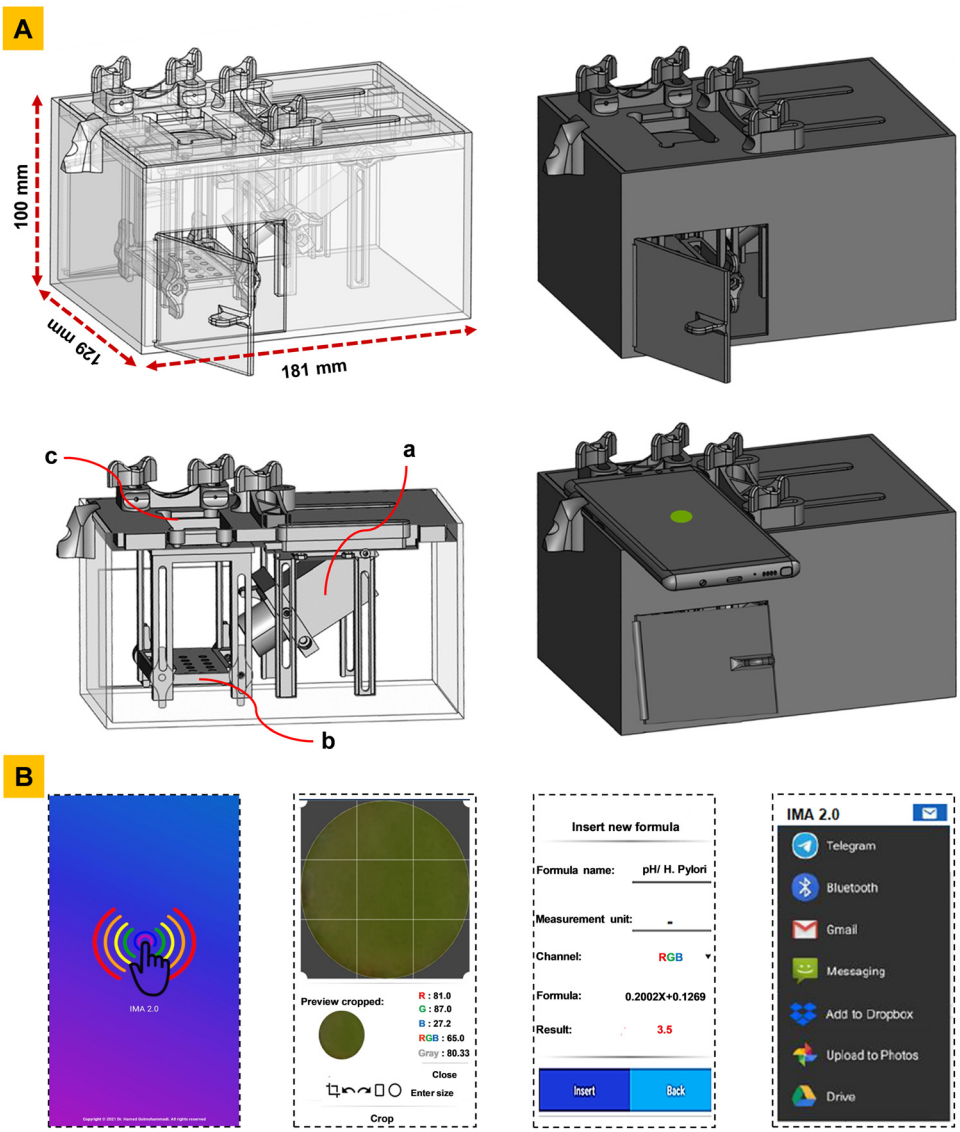

Fig. 2 (A) Illustration of the portable smartphone-based imaging platform laser setup (SIS) containing different parts: (a) an adjustable gradient structure equipped with a laser diode module, (b) an adjustable movable sample holder structure equipped with a glass-based strip with defined zones for sample placement, and (c) a circular chamber containing an optical UV/NIR cut-off filter and a hole for placing the smartphone's camera for capturing images. (B) Images of IMA (from left to right: IMA logo, the captured image of the sensor, the image processing/calculation view, and sharing data pathways).

gradient structure equipped with an infrared laser diode module, as an excitation source for UCNPs embedded in the fabricated fluorescent sensors, an adjustable movable sample holder structure equipped with a glass-based strip/slide with defined zones for the sample placement, a circular chamber containing an optical (UV)/NIR cut-off filter and a hole for the smartphone camera was first fabricated and the mentioned compartments were then fixed in their predetermined places. In order to take the fluorescence image of the fabricated ChNF paper-based sensors, they are placed within the dark chamber through a side strip hole, and the setup is subsequently integrated with the smartphone's camera. Furthermore, we used our developed android app (IMA) in order to quantify our nanosensor response. Fig. 2B demonstrates the different steps from imaging to analyzing and data sharing enabled by IMA. Apart from cost-effectiveness (Table S1, ESI†), ease of fabrication and use, and on-body monitoring capability compared to reported methods for the diagnosis of *H. pylori* infection, our fabricated smartphone-based imaging platform also benefits from fixed imaging conditions. It is noteworthy

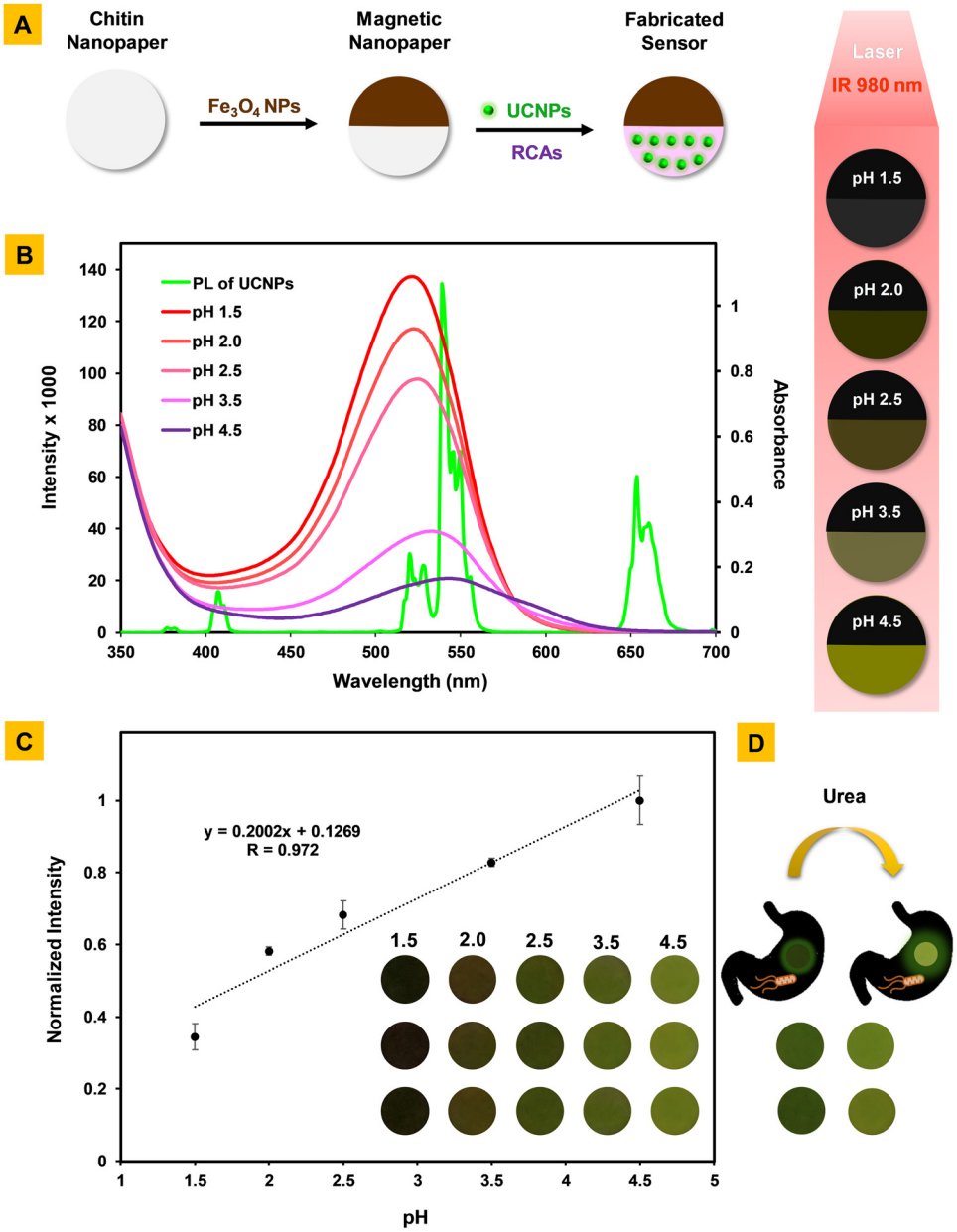

Fig. 3 (A) Schematic representation of the fabrication of the nanopaper-based sensor. (B) The relative spectral overlap between the emission spectrum of UCNPs and the absorbance spectra of RCAs and a schematic pH-dependent color/fluorescence profile of the fabricated sensor under 980 nm NIR irradiation in the pH range of 1.5 to 4.5. (C) The calibration curve and corresponding images for the fluorescence determination of pH in simulated gastric juice using the developed nanosensor. (D) Digital images of pH differentiation of the fabricated nanosensor before (left) and after (right) the addition of 2 μL urea (1.6 M) in simulated gastric juice including *H. pylori* (10^8 CFU mL^{-1}).

that one of the main drawbacks that significantly affects the accuracy and reliability of imaging-based optical sensors is the dependence of the analytical results obtained on the ambient light and the distance and angle of imaging, all of which have been well considered in the design of our developed imaging module.

Recommended sensing strategy for *H. pylori* infection diagnosis

The sensing strategy for the diagnosis of *H. pylori* infection using the developed sensor relies on the enzymatic reaction of *H. pylori* urease with urea and production of ammonia. The produced ammonia in turn *via* a mechanism called the ''inner filter effect'' (IFE) leads to variations in the pH-dependent color/fluorescence profile of the developed sensor. The IFE phenomenon refers to the absorption of the excitation and/or emission light of a fluorophore using an appropriate absorber, which results in the fluorescence quenching of the fluorophore due to the spectral overlap between the absorption (excitation) and/or emission bands of the fluorophore with the absorption band of the absorber.[53–56] In this work, as shown in Fig. 3B, the photoluminescence (PL) of the developed sensor is dynamically quenched in the pH range of 4.5 to 1.5 as a result of the relative overlap between the different absorption spectra of RCAs and the PL spectrum of UCNPs in the spectral region of 510–560 nm. Given the pH-dependency of RCAs and the attributed color/absorbance variations in different pHs, the PL of the developed sensor would be specific at each pH level. Accordingly, since the addition of urea to gastric juice by interacting with bacteria's urease can lead to ammonia production and subsequent pH change, the developed sensor is capable of diagnosing the *H. pylori* infection in a fast manner.

Analytical performance and applicability of the developed sensor for pH/*H. pylori* detection in simulated gastric juice: an *in vitro* study

In this work, the pH differentiation before and after the addition of urea is measured by SIS and considered as an output signal that is in relationship with the presence of *H. pylori* in media. Primarily, by considering the optimal concentrations of sensing elements (UCNPs and RCAs), the analytical characteristics of our sensor were assessed in simulated gastric juice. The calibration curve was plotted and showed a linear relationship in the pH range of 1.5–4.5 with a correlation coefficient of $r = 0.972$. The regression equation for pH was also $y = 0.2002x + 0.1269$, where y is the optical analytical signal (normalized RGB value) and x is the pH of the solution (Fig. 3C). Also, the relative standard deviation for seven replicate measurements of pH = 1.5 was 1.47, which confirms the reproducibility of our developed sensor. It should be highlighted that the fluorescence/color profile of our developed sensor in different pHs are in the range of dark to bright green, which can be easily screened even by the naked eye (Fig. 3C, inset image). What's more, by using the analytical characteristics of our pH-responsive sensor, it was employed for the diagnosis of *H. pylori* infection according to the recommended sensing strategy. The fluorescence/color profile of our sensor, as shown in Fig. 3D, well indicates that in the presence of *H. pylori* and urea, the pH of simulated gastric juice increases and reaches ~4, confirming its high efficiency for diagnosis of *H. pylori* infection.

Conclusions

Considering its high prevalence as one of the main causes of most digestive diseases, such as gastroduodenal ulcers, chronic active gastritis, and gastric cancer, the early diagnosis of *H. pylori* infection is of great significance. In this work, we have developed a nanopaper-based sensor for smart non-invasively diagnosis of *H. pylori* infection. The sensing elements consist of UCNPs and RCAs immobilized in the 3D scaffold of a magnetic nanopaper. The sensing strategy is based on the resulting pH differentiation before and after the addition of urea, which originates from the interaction of urea with *H. pylori*'s urease and production of ammonia. The resulting pH variations affected the color/fluorescence profile of our sensor, which was monitored using a smartphone-based laser imaging platform.

While somewhat effective, existing ITs for *H. pylori* infection diagnosis have several disadvantages, such as demanding endoscopy and multiple biopsies, costly and bulky apparatus, timely procedures, and professional labor to run and analyze the tests.[57,58] On the other hand, current NITs suffer from poor specificity, sensitivity, and reproducibility, and the use of relatively expensive laboratory equipment as well as harmful and isotopically labeled chemicals.[59,60] Meanwhile, due to the use of non-toxic materials (ChNF paper, RCAs, UCNPs and iron oxide NPs)[34,61] in the fabrication of our developed sensor, as well as the ease of fabrication and use, the relatively low price (Table S1, ESI†), the use of smartphone technology, and on-body monitoring capability, our sensing platform can potentially be exploited as an ingestible/wearable sensor for smart non-invasively diagnosis of *H. pylori* infection.

Furthermore, considering the high performance of our optical sensing platform for measuring pH in the range of 1.5 to 4.5, which was also validated by the *in vitro* study in simulated gastric juice, it can be utilized as an explicit sensor for pH monitoring of the GI tract to diagnose several pH-related upper GI diseases including hiatal hernia, gastritis, ulcers, gastro-esophageal reflux disease (GERD), *etc.*[62–66] In addition, our developed sensor by detecting gastric *H. pylori* infection during the treatment process can help specialists in its therapeutic monitoring.

A schematic overview of our proposed workflow on how our developed sensing platform can be employed as an ingestible/wearable sensor for on-body and non-invasive monitoring of gastric pH/*H. pylori* infection is shown in Scheme 1.

Altogether, owing to the results obtained from our developed sensor, we believe that such smart nanosensors can be potentially applicable for monitoring proteins, enzymes, hormones, metabolites, and microbial agents in gut lumen as well,

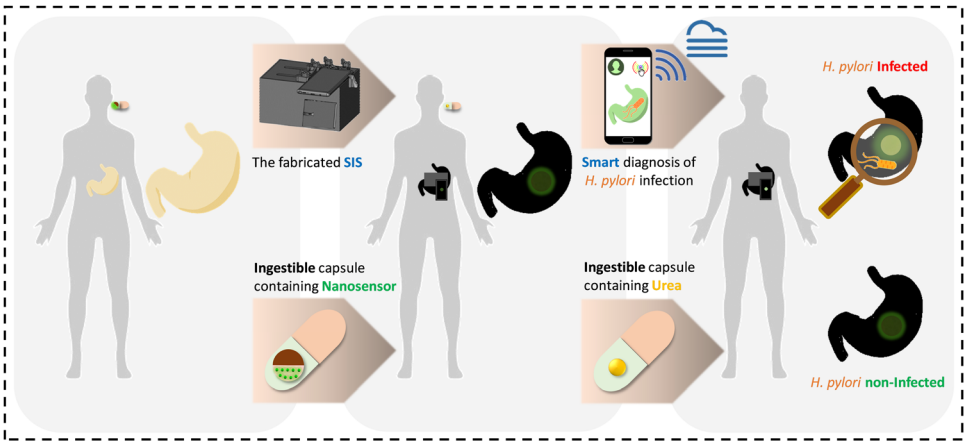

Scheme 1 A schematic overview of our proposed workflow on how to use our developed sensing platform for on-body and non-invasive monitoring of the gastric pH/*H. pylori* infection.

while inspiring the design and fabrication of innovative swallowable/ingestible sensors for non-invasive diagnosis of a variety of GI disorders/diseases.

Conflicts of interest

The authors declare no competing financial interests.

Acknowledgements

All authors gratefully acknowledge support from the Chemistry & Chemical Engineering Research Centre of Iran (Tehran, Iran), the University of Gorgan (Gorgan, Iran), the Shahid Beheshti University of Medical Sciences (Tehran, Iran), and the Czech Science Foundation (no. 21-04420S). H. G. would like to thank to the Alexander von Humboldt-Stiftung/Foundation for their financial support under the Georg Förster Research Fellowship Program.

Notes and references

1 J. Chen, S. M. Andler, J. M. Goddard, S. R. Nugen and V. M. Rotello, *Chem. Soc. Rev.*, 2017, **46**, 1272–1283.
2 M. S. Mannoor, H. Tao, J. D. Clayton, A. Sengupta, D. L. Kaplan, R. R. Naik, N. Verma, F. G. Omenetto and M. C. McAlpine, *Nat. Commun.*, 2012, **3**, 763.
3 A. K. Miller and S. M. Williams, *Genes Immunity*, 2021, **22**, 218–226.
4 J. Khatoon, R. P. Rai and K. N. Prasad, *World J Gastrointest. Oncol.*, 2016, **8**, 147.
5 P. Knezevic, V. A. Sabo, N. Simin, M. Lesjak and N. Mimica-Dukic, *J. Pharm. Biomed. Anal.*, 2018, **152**, 271–278.
6 K. Saxena, N. Chauhan and U. Jain, *Anal. Biochem.*, 2021, **630**, 114325.
7 I. A. Charitos, D. D'Agostino, S. Topi and L. Bottalico, *Gastroenterology Insights*, 2021, **12**, 111–135.
8 C.-Y. Kao, B.-S. Sheu and J.-J. Wu, *Biomedical J*, 2016, **39**, 14–23.
9 K. S. Bailey, H. E. Brown, V. Lekic, K. Pradeep, J. L. Merchant and R. B. Harris, *Helicobacter*, 2023, **28**, e12954.
10 H. Sung, J. Ferlay, R. L. Siegel, M. Laversanne, I. Soerjomataram, A. Jemal and F. Bray, *Ca-Cancer J. Clin.*, 2021, **71**, 209–249.
11 S. Salvatori, I. Marafini, F. Laudisi, G. Monteleone and C. Stolfi, *Int. J. Mol. Sci.*, 2023, **24**, 2895.
12 R. Ghotaslou, H. E. Leylabadlo and Y. M. Asl, *World J. Methodol.*, 2015, **5**, 164.
13 E. Tacconelli, E. Carrara, A. Savoldi, S. Harbarth, M. Mendelson, D. L. Monnet, C. Pulcini, G. Kahlmeter, J. Kluytmans and Y. Carmeli, *Lancet Infect. Dis.*, 2018, **18**, 318–327.
14 N. S. Atkinson and B. Braden, *Dig. Dis. Sci.*, 2016, **61**, 19–24.
15 A. I. Cardos, A. Maghiar, D. C. Zaha, O. Pop, L. Fritea, F. Miere and S. Cavalu, *Diagnostics*, 2022, **12**, 508.
16 A. Talebi Bezmin Abadi, *J. Pathog.*, 2018, **2018**, 9064952.
17 R. Nosrati, B. Golichenari, A. Nezami, S. M. Taghdisi, B. Karimi, M. Ramezani, K. Abnous and S. A. M. Shaegh, *TrAC, Trends Anal. Chem.*, 2017, **97**, 428–444.
18 E. Garza-González, G. I. Perez-Perez, H. J. Maldonado-Garza and F. J. Bosques-Padilla, *World J. Gastroenterol.*, 2014, **20**, 1438.
19 D. Y. Graham and M. Miftahussurur, *J. Adv. Res.*, 2018, **13**, 51–57.
20 T. Shimoyama, *World J. Gastroenterol.*, 2013, **19**, 8188.
21 E. M. McConnell, D. Morrison, M. A. R. Rincon, B. J. Salena and Y. Li, *TrAC, Trends Anal. Chem.*, 2020, **124**, 115785.
22 M. M. Ali, M. Wolfe, K. Tram, J. Gu, C. D. Filipe, Y. Li and J. D. Brennan, *Angew. Chem.*, 2019, **131**, 10012–10016.
23 Z. Liu and X. Su, *Biosens. Bioelectron.*, 2017, **87**, 66–72.
24 H. Yoo, H. Jo and S. S. Oh, *Mater. Adv.*, 2020, **1**, 2663–2687.
25 E. M. McConnell, I. Cozma, Q. Mou, J. D. Brennan, Y. Lu and Y. Li, *Chem. Soc. Rev.*, 2021, **50**, 8954–8994.
26 K. Kalantar-Zadeh, N. Ha, J. Z. Ou and K. J. Berean, *ACS Sens.*, 2017, **2**, 468–483.

27 L. A. Beardslee, G. E. Banis, S. Chu, S. Liu, A. A. Chapin, J. M. Stine, P. J. Pasricha and R. Ghodssi, *ACS Sens.*, 2020, **5**, 891–910.
28 E. De la Paz, N. H. Maganti, A. Trifonov, I. Jeerapan, K. Mahato, L. Yin, T. Sonsa-Ard, N. Ma, W. Jung and R. Burns, *Nat. Commun.*, 2022, **13**, 7405.
29 M. Mimee, P. Nadeau, A. Hayward, S. Carim, S. Flanagan, L. Jerger, J. Collins, S. McDonnell, R. Swartwout and R. J. Citorik, *Science*, 2018, **360**, 915–918.
30 K. Kalantar-Zadeh, K. J. Berean, N. Ha, A. F. Chrimes, K. Xu, D. Grando, J. Z. Ou, N. Pillai, J. L. Campbell and R. Brkljača, *Nat. Electron.*, 2018, **1**, 79–87.
31 C. J. Bettinger, *Angew. Chem., Int. Ed.*, 2018, **57**, 16946–16958.
32 T. Naghdi, H. Golmohammadi, H. Yousefi, M. Hosseinifard, U. Kostiv, D. Horak and A. Merkoci, *ACS Appl. Mater. Interfaces*, 2020, **12**, 15538–15552.
33 U. Kostiv, Z. K. Farka, M. J. Mickert, H. H. Gorris, N. Velychkivska, O. Pop-Georgievski, M. J. Pastucha, E. K. Odstrčilíková, P. Skládal and D. Horák, *Biomacromolecules*, 2020, **21**, 4502–4513.
34 U. Kostiv, V. Lobaz, J. Kučka, P. Švec, O. Sedláček, M. Hrubý, O. Janoušková, P. Francová, V. Kolářová and L. Šefc, *Nanoscale*, 2017, **9**, 16680–16688.
35 S. Pourjavaher, H. Almasi, S. Meshkini, S. Pirsa and E. Parandi, *Carbohydr. Polym.*, 2017, **156**, 193–201.
36 S. A. Jadhav and S. V. Patil, *Front. Mater. Sci.*, 2014, **8**, 193–198.
37 S. Malek, M. K. Pirouzifard, A. Yadegar, S. M. V. Bonab, B. Jannat and M. Moslemi, *Appl. Food Biotechnol.*, 2022, **9**, 321–331.
38 A. Nabavi-Rad, S. Jamshidizadeh, M. Azizi, A. Yadegar, K. Robinson, T. M. Monaghan and M. R. Zali, *Front. Cell. Infect. Microbiol.*, 2023, **13**, 529.
39 L. Bai, L. Liu, M. Esquivel, B. L. Tardy, S. Huan, X. Niu, S. Liu, G. Yang, Y. Fan and O. J. Rojas, *Chem. Rev.*, 2022, **122**, 11604–11674.
40 T. Naghdi, H. Yousefi, A. R. Sharifi and H. Golmohammadi, *Comprehensive analytical chemistry*, Elsevier, 2020, vol. 89, pp. 257–312.
41 A. R. Sharifi, T. Naghdi, H. Yousefi, M. A. Kiani and H. Golmohammadi, *ACS Sustainable Chem. Eng.*, 2022, 16995–17026.
42 E. M. Chan, *Chem. Soc. Rev.*, 2015, **44**, 1653–1679.
43 S. Wen, J. Zhou, K. Zheng, A. Bednarkiewicz, X. Liu and D. Jin, *Nat. Commun.*, 2018, **9**, 2415.
44 F. Wang, D. Banerjee, Y. Liu, X. Chen and X. Liu, *Analyst*, 2010, **135**, 1839–1854.
45 S. Ghosh, Y.-F. Chang, D.-M. Yang and S. Chattopadhyay, *Biosens. Bioelectron.*, 2020, **155**, 112115.
46 C. Ding, S. Cheng, C. Zhang, Y. Xiong, M. Ye and Y. Xian, *Anal. Chem.*, 2019, **91**, 7181–7188.
47 H. Chen, J. Yu, J. Zhang, K. Sun, Z. Ding, Y. Jiang, Q. Hu, C. Wu and D. T. Chiu, *Angew. Chem.*, 2021, **133**, 19480–19485.
48 T. Naghdi, S. Faham, T. Mahmoudi, N. Pourreza, R. Ghavami and H. Golmohammadi, *ACS Sens.*, 2020, **5**, 3770–3805.
49 S. Fang, Z. Guan, C. Su, W. Zhang, J. Zhu, Y. Zheng, H. Li, P. Zhao and X. Liu, *Food Control*, 2022, **138**, 109018.
50 N. Ghareaghajlou, S. Hallaj-Nezhadi and Z. Ghasempour, *Food Chem.*, 2021, **365**, 130482.
51 G. Hrazdina, *The flavonoids: advances in research*, 1982, 135–188.
52 R. E. Wrolstad, *Color and pigment analyses in fruit products*, Oregon State University, 1993.
53 M. Shafizadeh, S. Abbasi-Moayed, Z. Hamzei, A. Keshavarz, S. Yousefi, M. R. Hormozi-Nezhad and H. Golmohammadi, *Biosensors Bioelectronics: X*, 2022, **11**, 100150.
54 H.-R. Nan, Y.-H. Liu, W.-J. Gong, H.-B. Peng, Y.-Q. Wang, Z.-B. Zhang and X.-H. Cao, *Anal. Methods*, 2022, **14**, 532–540.
55 K. Ning, Y. Fu, J. Wu, Y. Sun, K. Liu, K. Ye, J. Liu, Y. Wu and J. Liang, *Anal. Methods*, 2023, **15**, 79–86.
56 E. Sheng, Y. Lu, Y. Tan, Y. Xiao, Z. Li and Z. Dai, *Anal. Chem.*, 2020, **92**, 4364–4370.
57 L. Chen, X. Li, T. Zou, T. Wang, X. Cui, Y. Chen, C. Zhang and S. Zhao, *Analyst*, 2019, **144**, 4086–4092.
58 K. Saxena, A. Kumar, N. Chauhan, M. Khanuja, B. D. Malhotra and U. Jain, *ACS Omega*, 2022, **7**, 32292–32301.
59 Y. Zilberman and S. R. Sonkusale, *Biosens. Bioelectron.*, 2015, **67**, 465–471.
60 H. Wu, L. Gu, X. Ma, X. Tian, S. Fan, M. Qin, J. Lu, M. Lyu and S. Wang, *ACS Omega*, 2021, **6**, 3771–3779.
61 U. Kostiv, H. Engstová, B. Krajnik, M. Šlouf, V. Proks, A. Podhorodecki, P. Ježek and D. Horák, *Front. Chem.*, 2020, **8**, 497.
62 J. E. Richter and J. H. Rubenstein, *Gastroenterology*, 2018, **154**, 267–276.
63 J. Gray and M. Shiner, *Gut*, 1967, **8**, 74.
64 P.-J. Lu, P.-I. Hsu, C.-H. Chen, M. Hsiao, W.-C. Chang, H.-H. Tseng, K.-H. Lin, S.-K. Chuah and H.-C. Chen, *World J. Gastroenterol.*, 2010, **16**, 5496.
65 A. Tenca, S. Massironi, D. Pugliese, D. Consonni, A. Mauro, F. Cavalcoli, M. Franchina, M. Spampatti, D. Conte and R. Penagini, *Neurogastroenterol. Motil.*, 2016, **28**, 274–280.
66 Y. Ning, S. Cheng, J.-X. Wang, Y.-W. Liu, W. Feng, F. Li and J.-L. Zhang, *Chem. Sci.*, 2019, **10**, 4227–4235.